THE JOURNAL OF PHYSICAL CHEMISTRY C

ARTICLE

pubs.acs.org/JPCC

Penetratin-Conjugated Gold Nanoparticles − Design of Cell-Penetrating Nanomarkers by Femtosecond Laser Ablation

S. Petersen,[‡] A. Barchanski,[‡] U. Taylor,[§] S. Klein,[§] D. Rath,[§] and S. Barcikowski*[,‡]

[‡]Laser Zentrum Hannover e.V., Hollerithallee 8, 30419 Hannover, Germany

[§]Institute of Farm Animal Genetics (FLI), Höltystrasse 10, 31535 Neustadt, Germany

Supporting Information

ABSTRACT: Gold nanoparticles (AuNPs) are promising imaging agents for the long-term visualization and tracing of intracellular functions because they bear outstanding optical properties and are fairly easily bioconjugated. However, the design of such multifunctional nanosystems might be limited by their bioavailability. Cell-penetrating peptides (CPPs) have been shown to be efficient molecular transporters with very few indices of cytotoxicity also in conjunction with nanoparticles. In this context, the current work aims to explore the approach of in situ conjugation during laser ablation in liquids for the design of CPP−NP conjugates at the example of penetratin-conjugated AuNPs. Because penetratin is positively charged at neutral pH, the conjugation process most likely differs from the previously reported coupling of oligonucleotides with their negatively charged phosphate backbone. Results reveal that penetratin is more efficiently bound to AuNPs, increasing the pH value of the ablation media, whereas the size and morphology of the bioconjugates function in terms of the penetratin concentration during the laser process. Probable underlying processes such as size quenching, aggregation, and laser-induced partial melting are assessed by the means of transmission electron microscopy and UV−vis spectroscopy. In a preliminary biological study, laser scanning confocal and transmission electron microscopy revealed a successful uptake of penetratin-conjugated AuNPs for the first time in up to 100% of coincubated cells within 2 h.

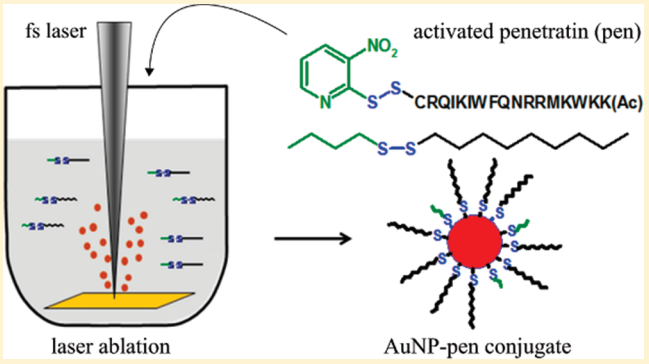

INTRODUCTION

The visualization and observation of physiological structures and cellular functions is vital for understanding, diagnosing, and treating diseases. Multifunctional nanosystems, composed of a combination of an inorganic core with a biomolecule shell, are reported to be promising imaging agents.[1] One inorganic core material with a high acceptance level in living systems is gold nanoparticles (AuNPs).[2] They feature unique optical properties including a strong surface plasmon resonance (SPR) with high quantum efficiency and resistance to photobleaching, making them visible by laser scanning confocal microscopy (LSCM)[3] and quantifiable down to the single particle level, even inside living cells.[4] The SPR maximum (SPR_{max}) can vary from 500 to 1000 nm in dependence of nanoparticle size, aspect ratio, and interparticle spacing. For example, the reduction of interparticle spacing during particle aggregation results in a red shift of SPR_{Max} due to interparticle plasmon coupling.[5] As a result, gold aggregates are easily excitable by near-infrared lasers within the optical window of blood and tissue; therefore, they might be used for visualization and simultaneous photothermal therapy of labeled sites.[6]

The functionalization of AuNPs can be achieved fairly easily via thiol linkers, resulting in a highly ordered self-assembled monolayer (SAM).[7] With this method, extracellular and intracellular targeting agents such as aptamers,[8] antibodies,[9] and effector molecules[10] are conjugable to the nanoparticle core.

However, the design of such multifunctional nanosystems might be limited by the question of their bioavailability, that is, their cellular uptake. In this context, molecular transporters with high uptake efficiency at low concentrations were discovered in the early 90s, when a series of short peptide sequences, known as protein transduction domains (PTDs), were identified to be able to efficiently cross cellular membranes.[11] Among these cell-penetrating peptides (CPPs), the most popular are Tat peptide and penetratin, derived from the human immunodeficiency virus type-1 (HIV-1) Tat (transactivator of transcription) and the *Drosophilia antennapedia* homeodomain (Antp) respectively. Both Tat and penetratin were shown to induce successful internalization of diverse biomolecules including DNA[12] and proteins.[13] Additionally, Tat and penetratin, conjugated to AuNPs via BSA[14,15] and

Special Issue: Laser Ablation and Nanoparticle Generation in Liquids

Received: September 30, 2010
Revised: December 7, 2010
Published: December 21, 2010

tiopronin[16] or polyethylene glycol spacer,[17] respectively, have already been described to deliver efficiently the nanoparticles into cells and even the nucleus.

However, probably because of the lack of rapid nanoparticle synthesis methods, enabling a fast design of nanoparticle bioconjugates with defined surface coverages, there are no studies screening the influence of the peptide concentration, the morphology of AuNPs, and further CPP on the internalization of nanoparticles. In previous studies, we established the in situ bioconjugation of AuNPs with thiolated single-stranded oligonucleotides during ultrashort pulsed laser ablation in liquids.[18] This one-step method allowed a rapid and simultaneous generation and conjugation of AuNPs with variable surface coverage values and bioconjugate sizes in dependence of the biomolecule concentration.[19] Here we explore this method for the design of CPP-conjugated gold nanoparticles at the example of the previously introduced penetratin (Pen: (Ac)NPys-CRQIKIWFQNRRMKWKK(Ac)), featuring a pyridyl disulfide (NPys) function at its N-terminal end with high affinity toward gold. Because penetratin is positively charged at neutral pH, the conjugation process most likely differs from the previously reported coupling of oligonucleotides with their negatively charged phosphate backbone. In this context, the preparation of cell-penetrating nanomarkers during laser ablation will be fundamentally analyzed with regard to conjugation efficiency as a function of peptide concentration and pH of the ablation media and bioconjugate size and morphology. Probable underlying effects are assessed by the means of transmission electron microscopy and UV−vis spectroscopy. Concerning later application prospects, we investigate the internalization efficiency of laser-generated AuNP−Pen bioconjugates into immortalized bovine endothelial cells in comparison with the direct internalization of ligand-free AuNPs for the first time.

EXPERIMENTAL METHODS

Generation and Bioconjugation of Gold Nanoparticles. Laser generation of gold nanoparticles was carried out using a femtosecond laser system (Spitfire Pro, Spectra-Physics) delivering 120 fs laser pulses at a wavelength of 800 nm (maximum energy: 400 μJ per pulse, beam diameter: 4 mm). The pulse energy and the distance of a 40 mm lens to the target's surface, referred to focal position, were fixed to 100 μJ and −1 mm at a repetition rate of 5 kHz. The focus in air is defined as the 0 focal position. The principle setup is described as follows: A 5 × 5 mm gold foil (thickness: 0.1 μm, purity >99.99%; Goodfellow GmbH) thoroughly cleaned was placed on the bottom in a well of a 48-well plate filled with 500 μL of double-distilled aqueous solution (ddH2O) of penetratin (0.0, 0.1, 0.5, 1, 5, 7.5, and 20 μM) (Scheme 1). The activated penetratin ((Ac)NPys-CRQIKIWFQNRRMKWKK(Ac)), featuring a pyridyl disulfide (NPys) function at its N-terminal end with high affinity toward gold, was purchased at MP Biomedicals. Because it has been previously reported that it is not necessary to disrupt the disulfide bond with a reducing agent to get self-assembly processes onto gold substrates,[26] the peptide was directly added to the ablation medium prior to the laser process. The well plate was then placed on an axis system that moved at a constant speed of 1 mm s^{-1} in a spiral with outer radius of 1 mm and inner radius of 0.4 mm. Time of irradiation was fixed to 106 s (corresponding to two spirals).

Bioconjugate Characterization. Zeta potential measurements were performed with the Zetasizer ZS (Malvern). In typical, 200 μL of the colloid were added to 800 μL water, and the resulting dilution was injected into the electrophoretic cell. Three consecutive measurements were carried out, and mean values are presented.

Scheme 1. In Situ Bioconjugation of AuNPs with the Cell-Penetrating Peptide Penetratin during Laser Ablation in Liquids

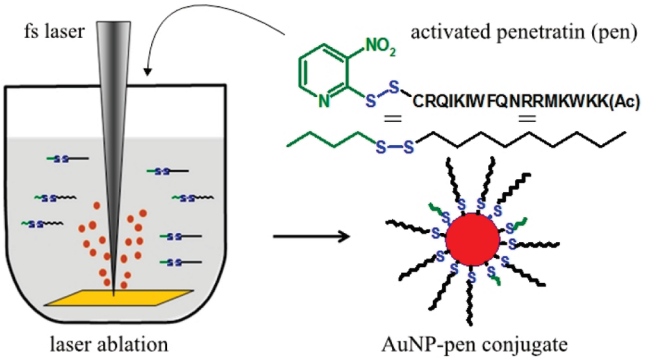

The conjugation efficiency was evaluated by the percentage of the total amount of peptide conjugated to AuNP. Therefore, the amount of unconjugated penetratin was measured by UV−vis spectroscopy (Shimadzu 1650) at 280 nm after separation of bioconjugates from remaining unconjugated penetratin by centrifugation for 30 min at 40 000*g*. Intensities were converted to molar concentrations by interpolation from a linear standard calibration curve. Standard curves were prepared with known concentrations of penetratin.

We obtained the average number of penetratin per AuNP by dividing the penetratin concentration, deduced by taking the difference of the total and the measured peptide concentration in the supernatant, by the original AuNP concentration. Therefore, we estimated AuNP mass concentrations by dividing the ablated mass, measured by weighing the gold foil three times prior and after ablation on a Sartorius balance (precision: 1 μg), by the used volume of ablation medium. Dividing this mass concentration by the average mass of one AuNP, which has been evaluated by means of TEM micrographs of at least 500 AuNPs, assuming spherical particles with a density equivalent to that of bulk gold (19.30 g cm^{-3}), yields the number concentration. We then calculated normalized surface coverage values by dividing the estimated particle surface area in the nanoparticle suspension.

MALDI-TOF of conjugates was performed at Stiftung Tierärztliche Hochschule, Rinderklinik (Prof. Dr. H. Bollwein, Dr. M. Ekhlase-Hundrieser) with Kratos Kompact MALDI 2. α-Cyano-4-hydroxycinnamic acid matrix (1 μL) was mixed with 1 μL of the sample and dried prior to analysis.

UV−vis spectra of the colloidal solutions were recorded in the spectral region 230−800 nm (Shimadzu 1650).

All transmission electron micrographs were registered at Stiftung Tierärztliche Hochschule, Institut für Pathologie (Prof. Dr. W. Baumgärtner, Kerstin Rohn) utilizing an EM 10 C electron microscope. In the case of the colloidal solution, one drop was placed on a carbon-coated, Formvar-covered copper grid and dried at room temperature. Given diameters are averaged over at least 500 AuNPs. The form factor (FF) is calculated by the following equation, $FF = 4\pi A/p^2$, where A is the area and p is the perimeter of each AuNP.

Cell Culture and Coincubation with Nanoparticles. The cells used in the studies were derived from a bovine immortalized endothelial cell line (GM7373[20]) obtained from the Cell Culture Collection, Institute of Infectology, FLI, Riems, Germany. All experiments were carried out in six-well dishes (TPP AG, Trasadingen, Switzerland). Cells were seeded in Dulbecco's modified Eagle's medium (DMEM; PAA Laboratories GmbH, Pasching, Austria) supplemented with 10% heat-inactivated fetal bovine serum (Invitrogen, Karlsruhe, Germany) and 1% penicillin/streptomycin (PAA Laboratories GmbH, Pasching, Austria) and allowed to attach and grow at 37 °C in a humidified 5% CO_2 atmosphere. After 24 h, new medium was added, this time, however, lacking the antibiotics. Following another 24 h, the medium was replaced again by DMEM alone or DMEM including AuNPs with or without Penetratin in a final concentration of 50 μM Au and then incubated for a further 2 h. All experiments were carried out in duplicate and repeated three times.

Cell Preparation for LSCM Analysis. In general, cell preparation for LSCM corresponded to previously described trials.[21] In short, after detachment and fixation in 0.5% paraformaldehyde (Merck KGaA, Darmstadt, Germany), cells were mixed 1:4 with Vectashield (Vector Laboratories, Burlingame, CA) and mounted on a slide within a paper reinforcement ring so as not to flatten the cells by the subsequently placed coverslip, which was fixed onto the slide with nail varnish. Visualization by LSCM was performed using an Axioplan 200 apparatus and a confocal imaging system LSM510 (Carl Zeiss MicroImaging GmbH, Jena, Germany) within the spectrum of visible light. A helium−neon-green laser of 543 nm was used to excite the SPR of the gold nanoparticles.

Cell Preparation for TEM Analysis. Cells to be used for TEM examinations were not detached but fixed adhered to the bottom of the six-well dishes with the aid of 2 mL of 2% glutaraldehyde (Sigma Aldrich, Schnelldorf, Germany) in Dulbecco's phosphate-buffered saline (PBS; Sigma-Aldrich Chemie GmbH, Steinheim, Germany), in which they remained at 4 °C until further processing. The thus-fixed cells were prepared for electron microscopy essentially as previously described[22] with slight modifications. In brief, the cell culture was rinsed in 0.1 M cacodylate buffer (pH 7.4), then postfixed in 1% (v/v) osmium tetraoxide, rinsed again in cacodylate buffer, dehydrated with increasing concentrations of ethanol, and subsequently embedded in Epon. The prepared cell layer was trimmed and processed for standard transmission ultrastructural examination.

RESULTS AND DISCUSSION

Conjugation Efficiency Is Defined by the pH Value of the Ablation Medium. Because the net charge of peptides and the charge of laser-generated AuNPs are dictated by the pH value of their environment,[23] conjugation efficiency will probably also function in dependence of the pH of the ablation medium.

Penetratin is highly positively charged at neutral pH contributed by basic residues of lysine (K) and arginine (R). The net charge of penetratin was calculated at various pHs based on the acid dissociation constants of the individual amino acids and the C-terminus (Figure 1a).[24] Because the N-terminus of the peptide is acetylated, there was no N-terminus included in calculating the pI of 12.8, and only the charged amino acids (K, R) and the C terminus contributed to the overall peptide charge.

The pH-dependent charge of AuNPs, generated under our experimental conditions, was estimated by ζ-potential measurements. The decay of the ζ potential with increasing pH (Figure 1a) confirms the data reported in the literature describing the partial oxidation of Au^0 to Au^+ and Au^{3+} and the successive association of dissociated water.[23,25] As a result, protonated hydroxyl groups ($-OH_2^+$), nonprotonated hydroxyl groups ($-OH$), and $-O^-$ are in equilibrium, whose relative abundance is dictated by the pH value of their environment. Under our experimental conditions, AuNPs hardly show any charge at pH <6; therefore, $-OH$ is dominant on the AuNPs surface leading to particle aggregation in the absence of stabilizing molecules because of the lack of efficient electrostatic stabilization. At pH ≥6, the abundance of $-O^-$ increases, and the AuNP global charge is getting increasingly negative.

The conjugation of AuNPs with penetratin was investigated at pH 6 to 9 to avoid repellence between AuNP and penetratin at low pH due to the presence of some protonated hydroxyl groups at the AuNP surface (zeta potential AuNP > 0 mV) and isoelectric point aggregation, precipitation of the peptide at elevated pHs, or both. Extreme pHs were further omitted to achieve better biocompatibility conditions already during bioconjugate synthesis and reduce purification steps for biological application.

An augmentation of conjugation efficiency, being defined as the percentage of total peptides bound to the AuNPs surface, could be observed with increasing pH value (Figure 1b). A possible explanation might be a dominant nonspecific electrostatic interaction of penetratin with AuNPs at lower pHs. At higher pH, the zeta potential of AuNPs is becoming increasingly more negative, which likely drives the positively charged penetratin to the AuNP surface, promoting dative binding via the sulfide to the gold core (Figure 1c). Mass spectrometry measurements (MALDI-TOF) of samples obtained in pH 9 reveal an increased second peak, having a mass difference of 155 Da compared with the molar mass of penetratin. This difference corresponds to the nitro-pyridyl sulfide residue, which is obviously more efficiently cleaved by the present gold nanoparticles at pH 9 compared with pH 6, confirming the assumption of an enhanced dative binding at higher pH (Figure S1 in Supporting Information). The formation of a mixed disulfide layer of peptide and nitro-pyridyl sulfide on the AuNPs surface might be the result, as previously reported for gold substrates in literature.[26] The following bioconjugates will be generated at pH 9.

The ζ potential of all bioconjugates shifted toward zero compared with ligand-free AuNPs generated at the same pH (Figure 1d). The ζ-potential difference increased from +7.4 mV at pH 6 to +16 mV at pH 9, correlating with the amount of conjugated positively charged penetratin.

Designing AuNP−CPP Bioconjugates varying the Penetratin Concentration. The design of AuNP−Pen bioconjugates was characterized after laser-based bioconjugation in aqueous solutions containing different amounts of penetratin at pH 9. Within <1 min of laser ablation, the ablation media were intensively colored, whereas a red shift of SPR_{max} with increasing penetratin concentration was observed (Figure 2). Because the nanoparticle concentration increases with penetratin concentration because of higher stabilization yields and less redeposition of ablated material,[18] UV−vis spectra have been normalized to an absorbance of 0.6 at 370 nm for better comparability.

To estimate the Feret diameter distribution and shape of the nanomarker, TEM micrographs were recorded, and size histograms were deduced for varied peptide concentrations in the ablation media (Figure 3: TEM images of bioconjugates generated in 0, 1, and 5 μM penetratin). Results reveal that there are probably three effects defining the bioconjugate size and aggregation

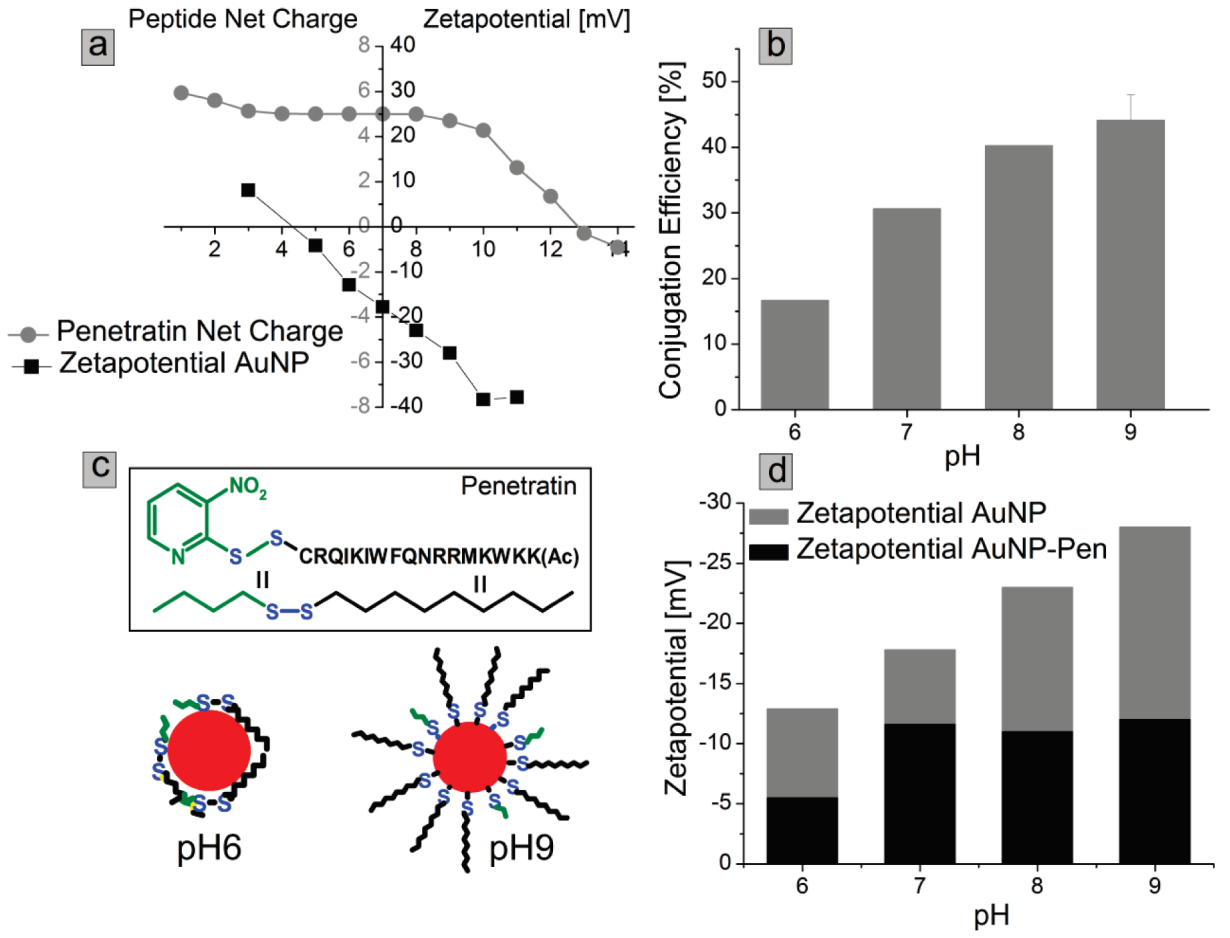

Figure 1. Conjugating AuNP with penetratin: (a) Calculated penetratin net charge and the measured zetapotential of AuNPs with varying pH values. (b) Percentage of added peptides (5 μM) conjugated to AuNPs increases with the pH of the laser ablation medium. (c) Estimated footprint of bioconjugates generated at pH 6 and 9. (d) Zeta potential of bioconjugates decreases in value with augmenting conjugation.

level at varied penetratin concentrations during laser ablation. Among these, the first mechanism is the documented and known size quenching effect, appearing during nanoparticle generation by laser ablation in liquids containing reactive molecules.[23,27]

Here AuNPs generated in water show the typical broad size distribution with an average Feret diameter of 15 nm, which decreases in the presence of penetratin to 6 nm (insert of Figure 4 and Table 1). Whereas no statistical difference in primary particle size has been observed, stability against aggregation could only be evidenced for nanoparticles generated in 0.1 to 1 μM penetratin by means of TEM micrographs and a negative zetapotential of <-25 mV despite the conjugation of positively charged penetratin. With an average AuNP concentration of 50 μg/mL generated in the presence of 1 μM penetratin, a stoichiometric ratio of inserted penetratin to AuNP of $\leq$32.5 seems to be required for stable primary nanoparticles. Because the surface coverage of penetratin per AuNP increases with the inserted concentration of penetratin, stable primary AuNPs can be obtained up to a maximal surface coverage. Under our experimental conditions, a maximal surface coverage of 27 penetratin molecules per stable primary AuNP was observed (Table 1).

Whereas AuNPs generated in 2.5 μM penetratin (Figure S3 in Supporting Information) already tend to aggregate, all AuNPs are aggregated in clusters of about 40−70 nm in diameter at penetratin concentrations $\geq$5 μM, referring to a stoichiometric ratio of 110 penetratin molecules per AuNP with an average AuNP concentration of 150 μg/mL (Figure 3).

This second effect seems more specific to peptide-like molecules because it is not observed during the conjugation of nucleic acids.[18] Because we observed more aggregation for higher peptide concentrations, the reason of "bridging" flocculation can be excluded. The cause might be more likely a reduction in electrostatic repulsions, which is confirmed by the lower ζ-potential value of bioconjugates with increasing peptide concentrations (Table 1 and Figure S2 of the Supporting Information). The shift in SPR_{max} follows the formation of aggregates and is probably dedicated to the decrease in the interparticle spacing (Figure 5).

The third effect occurs at penetratin concentrations >5 μM and results in the decrease in interparticle spacing and the deformation of spherical primary nanoparticles. (Detailed micrographs of bioconjugate aggregates generated in 5 and 20 μM of penetratin in TEM images in Figure 5.) This reshaping of primary particles probably results from a laser-induced partial melting and subsequent fusion of AuNPs with low interparticle distances in aggregates, as has been observed by Mafuné et al. during irradiation of a mixture of gold and platinum nanoparticles.[28] As a consequence, primary particle size, detected by TEM, seems to reincrease, whereas aggregate size decreases (Figure 4). For an estimation of the degree of particle deformation, we calculated the percentage of total AuNP in TEM micrographs having an FF

dx.doi.org/10.1021/jp1093614 |J. Phys. Chem. C 2011, 115, 5152–5159

value below 0.9. A perfect circle, characteristic for primary nanoparticles even when assembled in aggregates, has an FF of 1.0, whereas irregular structures like sintered particles deviate from unity toward zero as their degree of circularity become less perfect.[29] The resulting graph as a function of the peptide concentration correlates well with the described observations and interestingly also with the ratio of the absorbance at 800 nm to the absorbance at 380 nm of the SPR spectra (Figure 5). The absorbance at 800 nm is mainly due to asymmetric aggregates, whereas the absorbance at 380 nm is primarily caused by the interband transition of gold, which is a good parameter for the estimation of AuNP concentrations. However, for lower peptide concentrations, the correlation was deficient because estimation

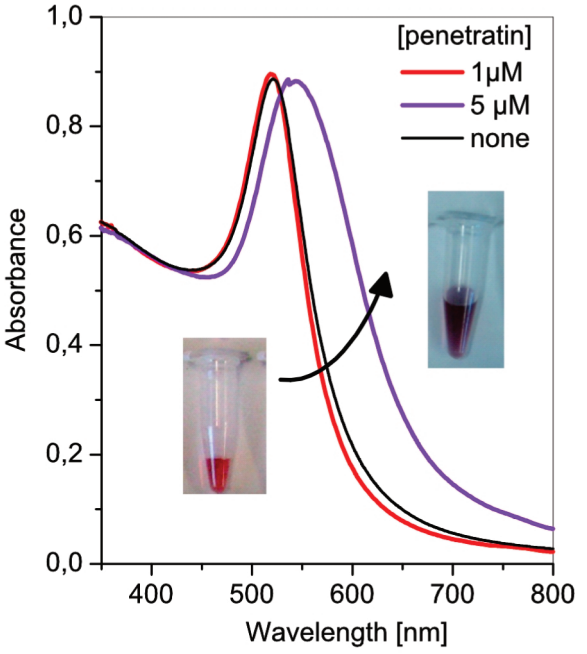

Figure 2. Normalized UV−vis spectra of ligand-free and penetratin-conjugated AuNP generated by laser ablation in water and in 1 and 5 μM penetratin solutions at pH 9.

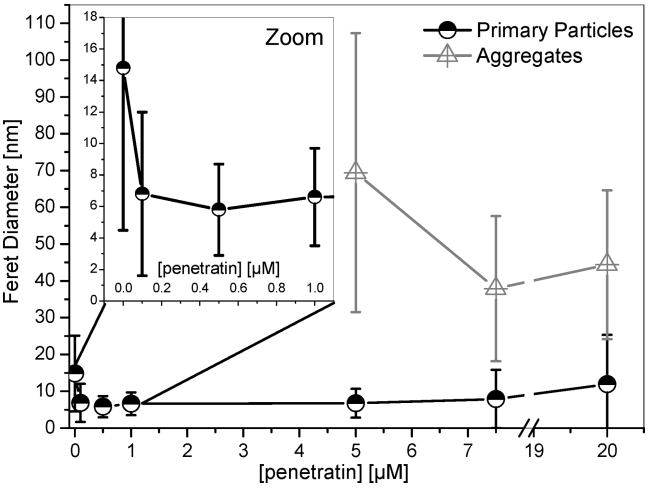

Figure 4. Influence of penetratin concentration on the Feret diameter (average diameter of primary particles and aggregates of AuNP−Pen

Table 1. Summary of Nanohybrid Surface Coverage and Particle Characteristics[a]

[penetratin] [μM]	$d_{F(NP)}$	$d_{F(Cluster)}$	zeta potential [−mV]	penetratin/NP
0	15 ± 10		28 ± 3	
0.1	7 ± 5		26 ± 1	10
0.5	6 ± 3		29 ± 1	24
1	7 ± 3		25 ± 1	27 ± 2
5	7 ± 4	69 ± 38	12 ± 2	43 ± 6
7.5	8 ± 8	38 ± 20	9 ± 5	74

[a] Values are means ± standard deviation.

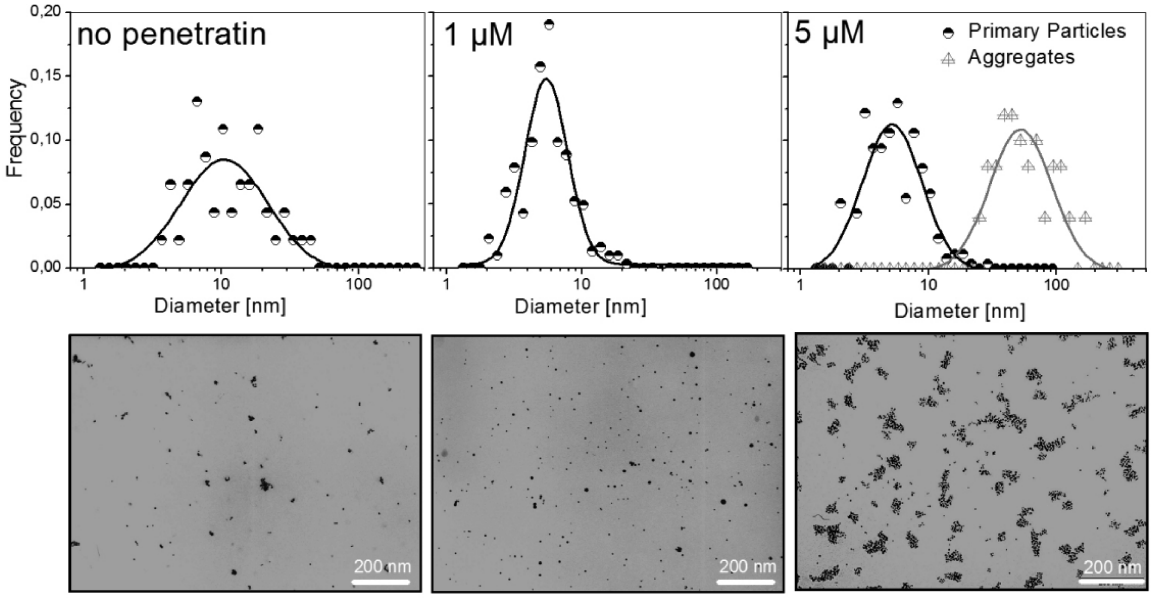

Figure 3. Influence of penetratin concentration on size and shape of the nanomarker: TEM histograms (top) and TEM images (bottom) of ligand-free and penetratin-conjugated AuNP generated by laser ablation in water and in 1 and 5 μM penetratin solutions at pH 9.

dx.doi.org/10.1021/jp1093614 |J. Phys. Chem. C 2011, 115, 5152–5159

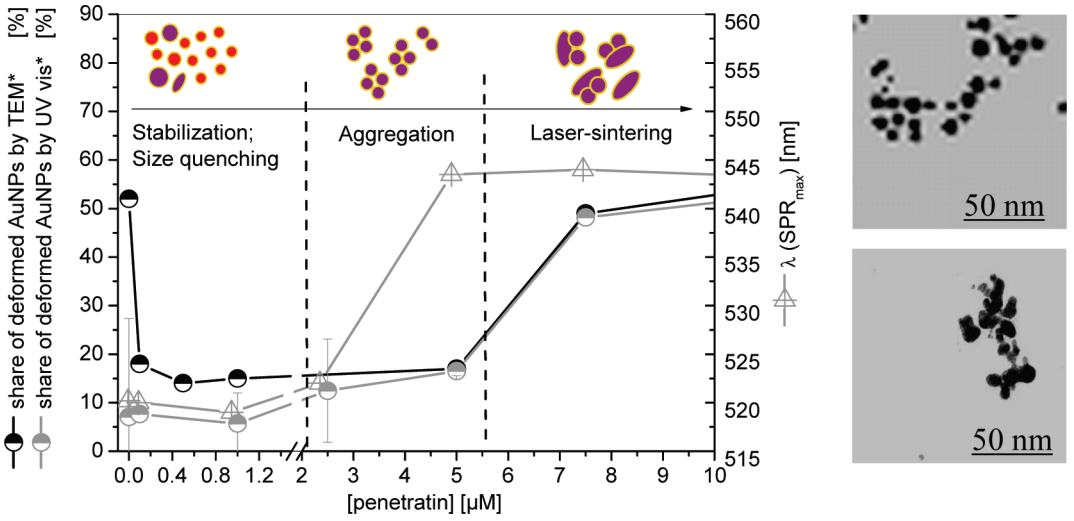

Figure 5. Share of deformed AuNPs, estimated by TEM and UV−vis spectroscopy, and shift in SPR_{max} in function of the penetratin concentration in the ablation medium at pH 9. *The share of deformed AuNPs, estimated by TEM micrographs, was defined as the share of AuNP with a form factor of <0.9. **The share of deformed AuNPs, estimated by UV−vis spectroscopy, was defined as the ratio of the absorbance at 800 and 380 nm. Right: TEM images of clusters generated in 5 (top) and 20 μM (bottom) penetratin. The interparticle spacing seems to decrease with higher peptide concentrations.

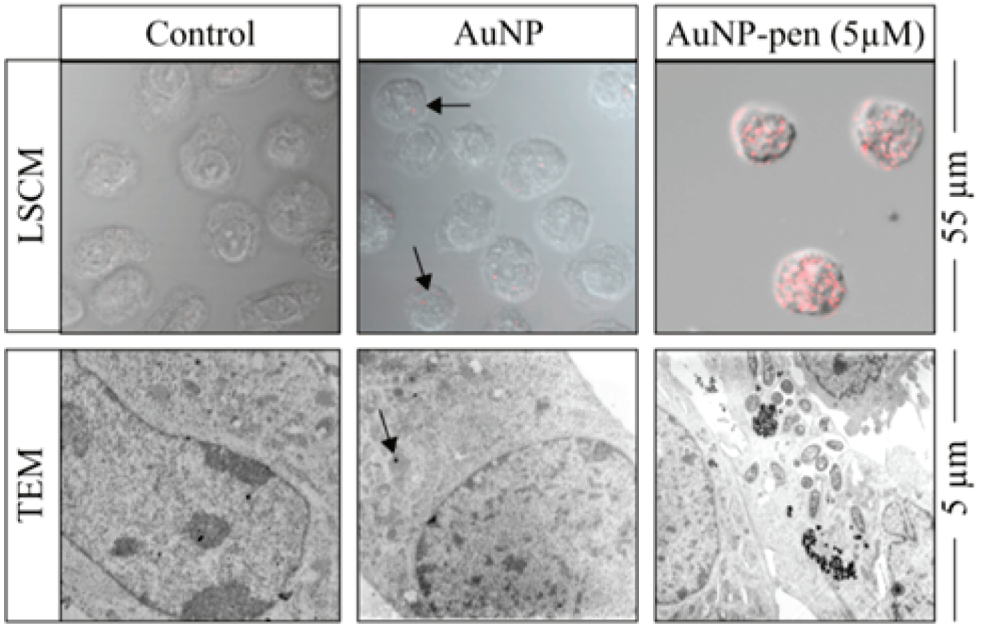

Figure 6. Influence of penetratin conjugation on cellular AuNP internalization: Representative laser scanning confocal microscopy images (top, red spots represent the backscatter of AuNPs after excitation at 543 nm) and transmission electron microscopy images (bottom) of immortalized bovine endothelial cells (GM7373); from left to right: negative controls, coincubation with AuNPs, and AuNP−penetratin conjugates for 2 h. The bioconjugates were generated by laser ablation in 5 μM penetratin.

by TEM analysis indicated a higher degree of deformed particles than the SPR spectra. Possibly AuNPs, generated in the absence or in the presence of a very low amount of penetratin, just show a low degree of aggregation in dispersion and form aggregates with overlapping nanoparticles on the TEM grid due to drying effects during the preparation for microscopic analysis and therefore mimic deformed particles.

In relevance to biological application, one can conclude that laser ablation enables the fast generation of penetratin-conjugated AuNPs with different levels of aggregation and penetration coverage by variation of the stoichiometric ratio of penetratin to AuNP. Both properties have been reported to determine cellular internalization. For instance, Lee et al. described the enhanced uptake of AuNP cluster compared with primary AuNPs of 15 nm in average diameter.[30] Additionally, AuNP aggregates exhibit higher scattering cross-section (Figure 2 and Figure S4 of the Supporting Information) and NIR absorption than primary gold nanoparticles Because the lower wavelength limit of the therapeutic window for in vivo diagnostics and photothermal therapy is ~640 nm, AuNP aggregates may be of promising use for the conversion of the absorbed NIR light into light scattering or localized heat. Moreover, particles that are bigger than the primary particles

dx.doi.org/10.1021/jp1093614 |J. Phys. Chem. C 2011, 115, 5152–5159

(6−10 nm) scatter light more efficiently and may hence be easily visualized by confocal microscopy and quantified down to the single particle level if the size exceeds 60 nm[4].

Cellular Internalization of Penetratin-Conjugated Gold Nanomarker. To gain a first insight into the cell-penetrating properties of femtosecond laser-generated AuNP−Pen nanomarker, we performed a 2 h coincubation of bovine endothelial cells with ligand-free AuNPs and AuNPs conjugated to penetratin by in situ conjugation during laser ablation in 5 μM penetratin. The so-achieved aggregates were assumed to be especially interesting for a first cell internalization study because of their good application prospects for in vivo diagnostics and photothermal therapy.

LSCM proved outstanding scattering properties of AuNP−Pen aggregates of 70 nm with an average surface coverage of 43 penetratin per each primary nanoparticle by determining SPR-enhanced light scattering at 543 nm with no photobleaching even after long-term irradiation.

Both incubations showed the successful internalization of AuNPs. However, the uptake efficiency seems to be significantly increased by penetratin conjugation. LSCM evidenced the presence of AuNPs in up to 100% of coincubated cells if the particles were penetratin-conjugated, whereas ligand-free AuNP were found in approximately half of the cells (Figure 6). TEM images underlined this fact. The penetratin conjugation apparently induces a different uptake mechanism: whereas ligand-free AuNPs diffused individually or in small clusters into the cells, as also previously observed by Salmaso et al.,[31] penetratin-conjugated AuNPs are accumulated in vesicles. The shape and surface coverage dependency of uptake efficiency and mechanism of laser-generated Au−Pen bioconjugates should be investigated in the future.

CONCLUSIONS

In situ conjugation during laser ablation allows the rapid design of cell-penetrating nanomarkers for intracellular bioimaging. Significantly enhanced penetratin conjugation efficiencies could be observed at higher pH values, whereas the size and morphology of bioconjugates depends on the peptide concentration during ablation. By means of MALDI-TOF measurements, the first effect could be attributed to a higher extent of specific dative binding of the penetratin's sulfide to the AuNP surface at increased pH. Probable underlying processes of size variation are defined as size quenching, aggregation, and laser-induced partial melting by means of transmission electron microscopy and UV−vis spectroscopy. A simple biological study during the recent work revealed a successful uptake of AuNP−Pen bioconjugates generated in 5 μM penetratin. Up to 100% of coincubated cells were marked with penetratin-conjugated AuNP within 2 h. In conclusion, AuNP conjugation to penetratin at higher biomolecule-to-nanoparticle ratios during laser ablation allows the fabrication of colloidal aggregates with about 40−70 nm diameter, which is in the size range that allows quantification of single nanoparticles in cells with confocal microscopy.

ASSOCIATED CONTENT

Supporting Information. Maldi-TOF spectra of penetratin after conjugation to AuNPs, zeta potential of bioconjugates versus penetratin concentration, TEM micrographs of AuNPs, and UV−vis spectra of ligand-free and penetratin-conjugated AuNP. This material is available free of charge via the Internet at http://pubs.acs.org.

AUTHOR INFORMATION

Corresponding Author

*E-mail: s.barcikowski@lzh.de. Tel: +49 511 2788 370. Fax: +49 511 2788 100.

ACKNOWLEDGMENT

The project was supported by the Masterrind GmbH Verden, the NBank Niedersachsen, and the excellence cluster REBIRTH. We thank Prof. Manstein and PD U. Curth (Medizinische Hochschule Hannover) for the possibility of using the centrifugation facilities, Dr. M. Ekhlasi-Hundrieser (Stiftung Tierärztliche Hochschule) for the MALDI TOF analysis of penetratin, Prof. Dr. W. Baumgärtner and Kerstin Rohn (Stiftung Tierärztliche Hochschule) for TEM analysis, and the Institute of Infectology, Friedrich Loeffler Institut, for providing cell culture collections.

REFERENCES

(1) Ted Thurn, K.; Brown, E. M. B.; Wu, A.; Vogt, A.; Lai, B.; Maser, J.; Paunesku, T.; Woloschak, G. E. *Nanoscale Res. Lett.* **2007,** *2,* 430.
(2) Lewinski, N.; Colvin, V.; Drezek, R. *Small* **2008,** *4,* 26.
(3) Sokolov, K.; Aaron, J.; Hsu, B.; Nida, D.; Gillenwater, A.; Follen, M. *Technol. Cancer Res. Treat.* **2003,** *2,* 491.
(4) Klein, S.; Petersen, S.; Taylor, U.; Rath, D.; Barcikowski, S. *J. Biomed. Opt.* **2010,** *15,* 036015.
(5) Link, S.; El-Sayed, M. *J. Phys. Chem. B* **1999,** *103,* 8410.
(6) Leo Ma, L.; Feldman, M. D.; Tam, J. M.; Paranjape, A. S.; Cheruku, K. K.; Larson, T. A.; Tam, J. O.; Ingram, D. R.; Paramita, V.; Villard, J.; Jenkins, T.; Wang, T.; Clarke, G. D.; Asmis, R.; Sokolov, K.; Chandrasekar, B.; Milner, T. E.; Johnston, K. P. *ACS Nano* **2009,** *3,* 2686.
(7) Alivisatos, A. P.; Johnsson, K. P.; Peng, X.; Wilson, T. E.; Loweth, C. J.; Bruchez, M. P.; Schultz, P. G. *Nature* **1996,** *382,* 609.
(8) Medley, C. D.; Smith, J. E.; Tang, Z.; Wu, Y.; Bamrungsap, S.; Tan, W. *Anal. Chem.* **2008,** *80,* 1067.
(9) Karyakin, A. A.; Presnova, G. V.; Rubtsova, M. Y.; Egorov, A. M. *Anal. Chem.* **2000,** *72,* 3805.
(10) Rosi, N. L.; Giljohann, D. A.; Thaxton, C. S.; Lytton-Jean, A. K.; Han, M. S.; Mirkin, C. A. *Science* **2006,** *312,* 1027.
(11) Derossi, D.; Joliot, A. H.; Chassaing, G.; Prochiantz, A. *J. Biol. Chem.* **1994,** *269,* 10444.
(12) Astriab-Fischer, A.; Sergueev, D.; Fischert, M.; Shaw, B. R.; Juliano, R. L. *Pharm. Res.* **2002,** *19,* 744.
(13) Fawell, S.; Seery, J.; Daikh, Y.; Moore, C.; Chen, L. L.; Pepinsky, B.; Barosoum, J. *Proc. Natl. Acad. Sci. U.S.A.* **1994,** *91,* 664.
(14) Tkachenko, A. G.; Xie, H.; Coleman, D.; Glomm, W.; Ryan, J.; Anderson, M. F.; Franzen, S.; Feldheim, D. L. *Bioconjugate Chem.* **2003,** *125,* 4700.
(15) Tkachenko, A. G.; Xie, H.; Liu, Y.; Coleman, D.; Ryan, J.; Glomm, W. R.; Shipton, M. K.; Franzen, S.; Feldheim, D. L. *Bioconjugate Chem.* **2004,** *15,* 482.
(16) Fuente, J. M.; Berry, C. C. *Bioconjugate Chem.* **2005,** *16,* 1176.
(17) Nativo, P.; Prior, I. A.; Brust, M. *ACS Nano* **2008,** *2,* 1639.
(18) Petersen, S.; Barcikowski, S. *Adv. Funct. Mater.* **2009,** *19,* 1167.
(19) Petersen, S.; Barcikowski, S. *J. Phys. Chem. C* **2009,** *113,* 19830.
(20) Schares, G.; Meyer, J.; Barwald, A.; Conraths, F. J.; Riebe, R.; Bohne, W.; Rohn, K.; Peters, M. *Int. J. Parasitol.* **2003,** *33,* 229.
(21) Grinspan, J. B.; Mueller, S. N.; Levine, E. M. *J. Cell. Physiol.* **1983,** *114,* 328.
(22) Taylor, U.; Klein, S.; Petersen, S.; Kues, W.; Barcikowski, S.; Rath, D. *Cytometry, Part A* **2010,** *77,* 439.
(23) Sylvestre, J. P.; Poulin, S.; Kabashin, A. V.; Sacher, E.; Meunier, M.; Luong, J. H. T. *J. Phys. Chem. B* **2004,** *108,* 16864.
(24) Cox, N. In *Lehninger Biochemistry*; Springer: Berlin, 2009; Vol. 4, Ch. 5.

(25) Muto, H.; Yamada, K.; Miyajima, K.; Mafuné, F. J. *J. Phys. Chem. C* **2007,** *111*, 17221.
(26) Lee, W.; Lee, D. B.; Oh, B. K.; Lee, W. H.; Choi, J. W. *Enzyme Microb. Technol.* **2004,** *35*, 678.
(27) Mafune, F.; Kohno, J.; Takeda, Y.; Kondow, T.; Sawabe, H. *J. Phys. Chem. B* **2001,** *105*, 5114.
(28) Mafuné, F.; Kohna, J.; Takeda, Y.; Kondow, T. *J. Am. Chem. Soc.* **2003,** *125*, 1686.
(29) Cox, E. J. *J. Paleontol.* **1927,** *1*, 179.
(30) Lee, S. H.; Bae, K. H.; Kim, S. H.; Lee, K. R.; Park, T. G. *Int. J. Pharm.* **2008,** *364*, 94.
(31) Salmaso, S.; Calicati, P.; Amendola, V.; Meneghetti, M.; Magnusson, J. P.; Pasparakis, G.; Alexandre, C. *J. Mater. Chem.* **2009,** *19*, 1608.